IAEA FUMAC BENCHMARK ON KIT BUNDLE TEST CORA-15

J. STUCKERT
Institute for Applied Materials, Karlsruhe Institute of Technology (KIT)
Hermann-von-Helmholtz-Platz 1, 76344 Eggenstein-Leopoldshafen, Germany

H. AUSTREGESILO, TH. HOLLANDS
Gesellschaft für Anlagen und Reaktorsicherheit (GRS) gGmbH
Boltzmannstrasse 14, 85748 Garching, Germany

A. KISELEV
Nuclear Safety Institute (IBRAE), Russian Academy of Sciences
B. Tulskaya 52, 115191 Moscow, Russian Federation

ABSTRACT

In framework of the FUMAC/IAEA project, a benchmark has been performed on the CORA-15 bundle test performed at KIT. Two organizations have provided results for this modelling: GRS/Germany (ATHLET-CD code applied) and IBRAE/Russia (SOCRAT code applied). In the test, the behaviour of the PWR type fuel bundle, composed of 23 fuel rods and 2 absorber rods, was investigated under severe accident conditions. An important feature of the experiment in difference to all other CORA bundle tests was the pressurization of fuel rods to 6 MPa. As a result, the fuel rods underwent ballooning and burst. In general, both codes adequately reproduced the cladding temperatures evolutions, its ballooning and rupture, and the blockage formation due to melt relocation. The hydrogen release has been calculated within the uncertainty of the measured data.

1. Introduction

The CORA experimental program at the Karlsruhe Institute of Technology (KIT, formerly KfK - Kernforschungszentrum Karlsruhe) was conducted between 1987 and 1993 [1]. Its main objective was to investigate the integral behaviour of typical light water reactors (LWR) fuel bundles under severe accident conditions. The bundle tests were performed out-of-pile and the decay heat was simulated by electrical heating. The test bundles contained all materials normally used in LWR fuel elements: UO_2 pellets, Zircaloy-4 fuel rod claddings, grid spacers, Ag-In-Cd absorber rods with stainless steel claddings and guide tubes were typical to those of commercial LWRs concerning their composition and radial dimensions. The CORA-15 test was performed with a bundle made up of 23 fuel rods and 2 absorber rods. The materials and radial dimensions of the fuel and absorber rods were identical to those in a PWR bundle. The fuel rods were pressurized to 6 MPa while the system pressure was 0.22 MPa to provoke a pronounced cladding ballooning and burst. The test scenario comprised the bundle heating in a steam-argon flow up to a temperature of ≈2100 °C followed by its cooling down in an argon flow. The temperature scenario simulates anticipated severe accident conditions in LWR core during small break LOCA.

Test has been simulated with the GRS system code ATHLET-CD, using as far as possible the same code input parameters and modelling options as for the simulation of a similar experiment, CORA-13, object of an OECD/NEA international standard problem (ISP-31) [2]. Afterwards, the input data set has been adapted for CORA-15 (initial and boundary conditions), using the same nodalization and as far as possible the same modelling options. The simulation of CORA-15 has been complemented by some additional sensitivity studies concerning the cladding rupture model options.

The aims of CORA-15 modelling by integral SOCRAT code are twofold: one is to investigate the ballooning effect on the bundle degradation, and the second is to validate CROX model to predict cladding ballooning and burst parameters, PROF and LIQF models to predict Zr

oxidation and hydrogen release, DROG model to predict melt relocation and blockage formation, and their interaction.

2. Experimental results

2.1. Description of the test facility

In the axial cross section of Fig. 1 the main components of the CORA facility are shown schematically. The facility is described in detail in [3] and [4]. Many details on the CORA-15 test can be found in [5]. The test rods were arranged within the CORA-15 bundle as shown in the schematic cross section of Fig. 2. 16 of the 25 fuel rods were electrically heated by using tungsten pins with length of 1.0 m as heater elements. The heated rods (fuel rod simulators) were filled with annular UO_2 pellets whereas the unheated rods contained full UO_2 pellets of the same outer diameter. Additionally, two absorber rods were installed. Composition characteristics of the CORA-15 bundle are presented in Table 1.

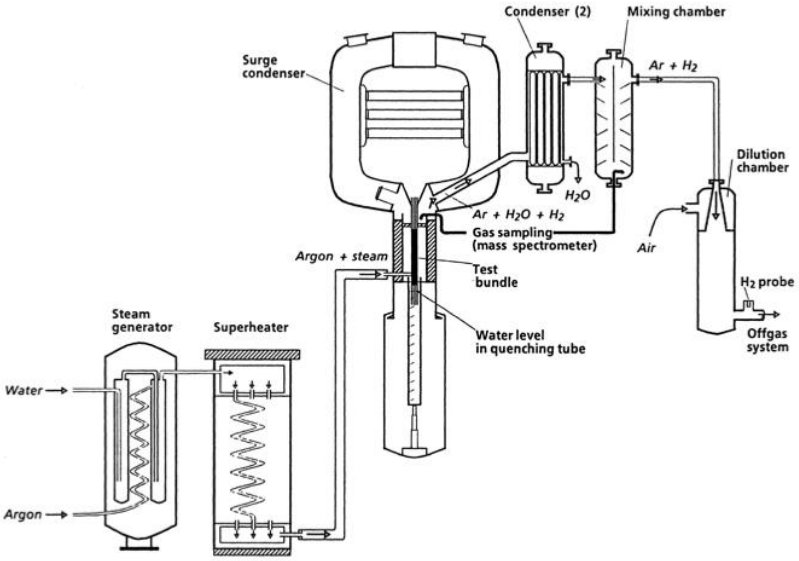

Fig 1. Main components of the CORA facility.

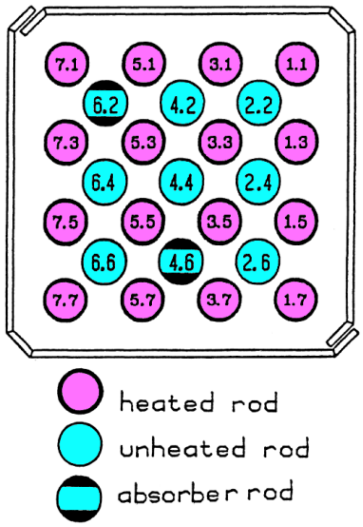

Fig 2. Cross section of CORA-15 bundle, top view.

The heated and unheated rods are mounted at the upper bundle flange and kept in place laterally by three grid spacers. The CORA shroud, a Zircaloy liner with about 20 mm thick ZrO_2 fibre insulation at the outside, surrounds the bundle. This fibre insulation extends only up to 1.0 m, and above this elevation - in the upper electrode zone - the shroud is not insulated in order to prevent the electrodes made of molybdenum and copper from melting. For optical on-line inspection, the shroud has several observation holes. The bundle could be observed by on-line optical inspection with several video systems along the test section. Six videoscopes were used in tests to observe the materials behaviour and the relocation of material during transient testing: at 30° (500 mm), 120° (400, 600, 800 mm), 120° (700 mm), 300° (900 mm). Based on these data, detailed analyses on melt relocation and damage progression could be made.

The test section was instrumented with thermocouples and two-colour pyrometers to measure steam temperature, rod cladding temperature, shroud temperature, and insulation temperature. The high-temperature thermocouples were made of W5Re/W26Re wires, insulated with HfO_2 and sheathed in Ta/Zry duplex tubing. For the positions at lower temperatures NiCr/Ni thermocouples with Inconel sheath were installed. For unheated rods, the thermocouples were installed in pellet centres, whereas for heated rods at the cladding outer surface.

The thermocouple wire accuracies (“limits of error”) are:

at bundle elevations between 0 and 500 mm (*NiCr/Ni thermocouples*): ± 2 K (up to 600 K), ± 0.005*T K (above 600 K);
at bundle elevations between 600 and +1300 mm (*W/Re thermocouples*): ± 5 K (up to 700 K), ± 0.01*T K (above 700 K).

However, the uncertainties of temperature measurements are usually higher because of additional uncertainty sources (TC connector, extension cable etc.) with TC mounting error as a main contributor.

Bundle size			25 rods
Number of heated rods			16
Pitch			14.3 mm
Rod outside diameter			10.75 mm
Cladding material			Zircaloy-4
Cladding thickness			0.725 mm
Rod length			2175 mm
Heated length			1000 mm
Fuel pellets	heated rods		UO_2 annular pellets
	unheated rods		UO_2 full pellets
U-235 enrichment			0.2 %
Pellet outer diameter (nominal)			9.1 mm
Heater material			Tungsten (W)
Heater diameter			6 mm
Grid spacer	material		Zircaloy-4, Inconel 718
	length		Zry 42 mm; Inconel 38 mm
	location	lower (Zry)	-5 mm*
		centre (Inc.)	+496 mm
		top (Zry)	+880 mm
Shroud	material		Zircaloy-4
	wall thickness		1.2 mm
	outside dimensions		86 x 86 mm
	elevation		36 mm…1236 mm
	insulation material		ZrO_2 fibre
Absorber rod	insulation thickness		20 mm
	number of rods		2
	material and composition		80Ag, 15In, 5Cd (wt.%)
	cladding		stainless steel
	cladding OD		10.2 mm
	cladding ID		8.85 mm
	length		1489 mm
	elevation		-189 mm to +1300 mm
Absorber rod guide tube	material		Zircaloy-4
	OD		13.8 mm
	wall thickness of tube		0.8 mm

*elevations are referred to the bottom of the heated zone

Tab 1. Design characteristics of the CORA-15 bundle.

The hydrogen produced during the test by the steam/Zr reaction was measured at two different positions that one can see in Fig. 1: 1) immediately above the test section (1st mass spectrometer) and then 2) in the mixing chamber after condenser. To dilute the gas taken at the location above the test section a dilution chamber with flow meters was installed. The off-gas mixtures which contain hydrogen among other gases were transported to the spectrometers via capillary tubes. Two quadrupole mass spectrometers of the type Leybold PQ 100 were used. The ion currents representing the concentrations of the respective gases are determined. From these data the mass production rate of hydrogen as well as of the other gases is calculated with the ratio of the partial pressure of the particular gas and that one of argon (carrier gas) and multiplied by the argon flow rate through the test bundle.

2.2. Test conduct and results of online measurements

In the CORA experiments the test sequence can be distinguished in the following phases:

Pre-heating	0000-3000 s (argon only),
Heat-up	3000- 3900 s (argon + steam),
Escalation	3900 - 4900 s (argon + steam),
Cool-down	≈ 4900 s (argon only).

After the pre-heating phase, the bundle was heated electrically at initial heat-up rate of 0.2 to 1 K/s in a mixture of steam and argon flow. Maximum temperatures of about 2100 °C were attained. At the end of a test, the hot bundle was slowly cooled down by argon. The power input history for the CORA-15 test together with the coolant data as argon flow, steam flow (provided as mass flow of the injected water into the evaporator), and system pressure are depicted in Fig. 3.

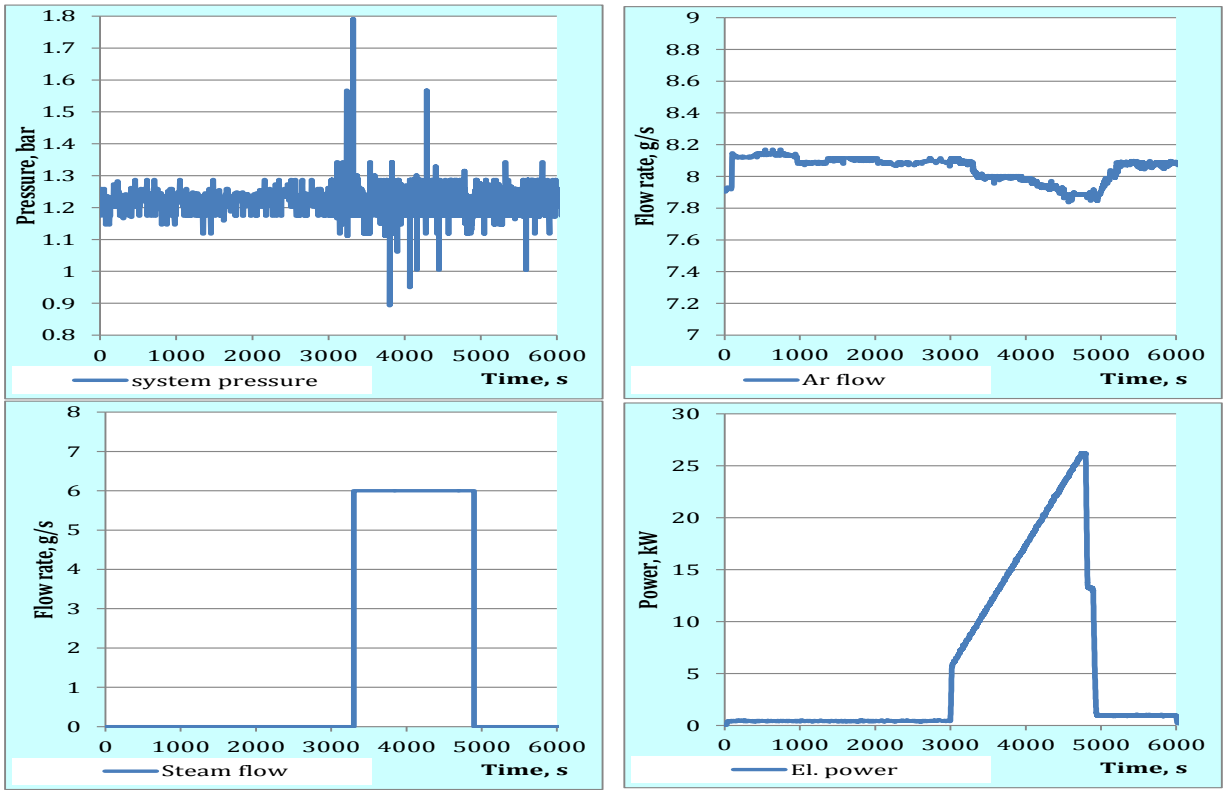

Fig 3. System pressure, argon flow, steam flow and electrical power of CORA-15.

The fuel rod simulators (heated and unheated) were initially pressurized to 6.0 MPa. All rods underwent ballooning and burst during the subsequent transient (Fig. 4). The ballooning started at about 650 °C and lasted about 100 s. The sequence of the burst for the individual rods is presented in Table 2.

rod	**5.1**	**3.3**	**3.5**	**1.3**	**5.5**	**5.3**	**2.4**	**3.1**	**1.1**
time, s	3493.8	3547.8	3561.5	3562.1	3562.7	3564.2	3565.1	3570.2	3579.4
rod	**7.5**	**7.3**	**1.5**	**5.7**	**7.7**	**7.1**	**4.4**	**3.7**	**6.4**
time, s	3579.5	3585.1	3588.7	3588.9	3593.9	3600.8	3600.9	3602.0	3602.2
rod	**4.2**	**2.2**	**1.7**	**2.6**	**6.6**				
time, s	3604.0	3616.3	3617.8	3624.8	3644.5				

Tab 2. Burst times.

Burst occurred within 150 s (from 3500 to 3650 s) in the temperature bandwidth between about 700 to 800 °C for majority of the rods (burst from 3550 to 3650 s). These temperatures were registered with the cladding TC between elevations 350 and 950 mm. The hottest

elevation during the burst time period was around the elevation 750 mm. It could be suggested that it was the burst axial position of the majority of rods. Uncertainties of the measured burst temperatures and elevations are discussed below in the chapter devoted to the test simulations.

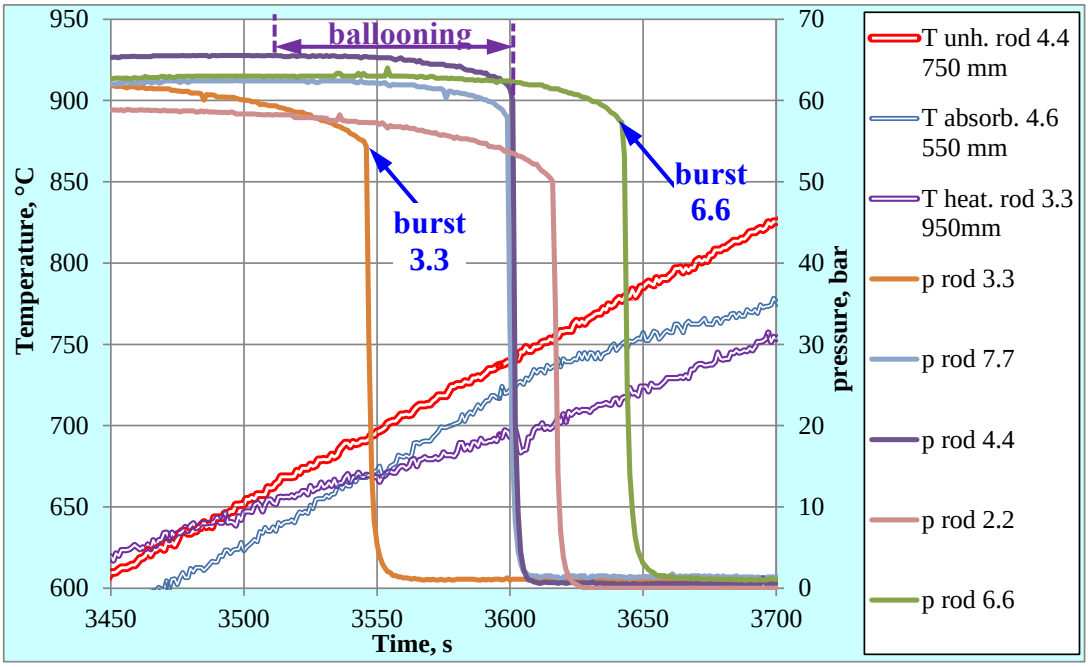

Fig 4. Ballooning and burst (readings of pressure transducers)

The readings of thermocouples during the test at two hot elevations are provided with Fig. 5. This figure shows also the readings of two pyrometers installed at elevations 690 and 890 mm and oriented to the bundle through holes in fibre insulation and shroud. Significant oscillations of thermocouple and pyrometer readings are connected to the Zry melt onset at T > 1760 °C. It could be suggested that after these incidences the thermocouples failed or were shifted to lower elevations. However, the comparison of thermocouple and pyrometer data at 750 and 950 mm shows very similar behaviour after oscillation occurrences. So, it can indicate the correctness of thermocouple readings also during the cooling stage.

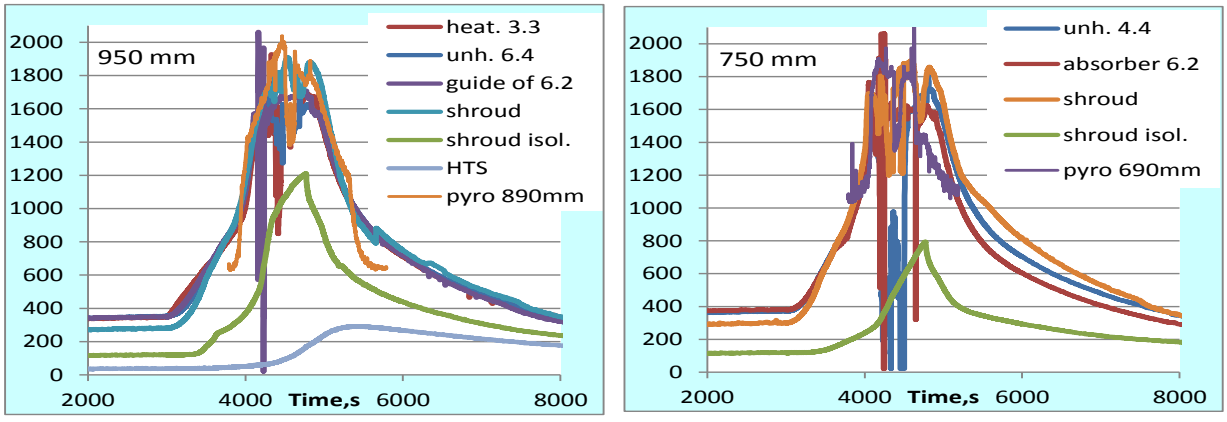

Fig 5. Thermocouple (and pyrometer) readings at two hot elevations of CORA-15 (temperature in °C)

The maximum temperature reached in the test amounts to about 2000 °C. The temperatures of absorber rod and pertinent guide tube show basically the same behaviour as the unheated or heated rods. A difference in CORA-15 compared to experiments without internal rod

pressure can be found for the temperature escalation process. In CORA-15 the escalation developed in the upper half of the bundle only. Usually the escalation also takes place in the lower half of the bundle, down to about 150 mm. Due to cladding ballooning and corresponding increase of the gap between pellet and cladding, the temperature in the lower part of the CORA-15 bundle was insufficient to trigger a temperature escalation.

The measured hydrogen data are derived from the ion current obtained from the gas probes 1) at the outlet of the test section (before condenser) and 2) at the outlet of the mixing chamber (after condenser). Both mass spectrometers indicate the maximum of the hydrogen release rate, about 210 mg/s, at the end of the transient. There is some time shift of the readings of the second mass spectrometer due to its larger distance from the bundle outlet. The total hydrogen release at the end of the test was 180 g according to the first mass spectrometer (installed before condenser) and 145 g according to the second mass spectrometer (installed after condenser). The data of the second spectrometer are more reliable due to absence of condensable gases (steam) at the measurement point. Due to problems with the pre-test calibration of spectrometers, the following measurement errors concerning the total hydrogen value could be estimated: ±20% for the first spectrometer and ±10% for the second mass spectrometer.

2.3. Post-test investigations

Metallographical investigations showed negligible oxidized cladding up to elevation of about 350 mm. The claddings were completely oxidized between elevations 480 and 1000 mm (Fig. 6). Larger cladding portions are missing. However, the pellet stacks of the full-pellet rods are kept in place. According to thermocouple readings, temperature escalation took place only in the upper half of the bundle. The post-test appearance confirms the result indicated by the temperature recordings. So, melting and relocation of material took place only in the upper half of the bundle. The absorber melt release occurred between 1290 and 1350 °C at elevations between 750 and 800 mm. Most of the melt reacts with the Zircaloy cladding and guide tube by liquefying the zirconium components, forming a metallic melt of the type (Ag, In, Zr). Due to its zirconium content this melt is capable of dissolving UO_2 as low as 1250 °C, i.e. clearly below the melting point of Zircaloy (1760 °C). During the temperature escalation above 1800 °C, Zr melt formed in the gap between ZrO_2 and UO_2 penetrated partially through the failed ZrO_2 layer into the space between rods. The resulting melt can be significantly oxidized, what was detected by single effect tests [6] and observed in many bundle tests [7]. Based on these results, the mechanistic model of the molten pool oxidation [8] and the model for melt blockage (slug) relocation with concurrent oxidation [9] were developed. In the CORA-15 test, the oxidized melt was solidified between 400 and 550 mm. A partial flow channel blockage occurred at elevations between 200 and 600 mm, i.e. below and upper the central grid spacer located at 496 mm (Fig. 7).

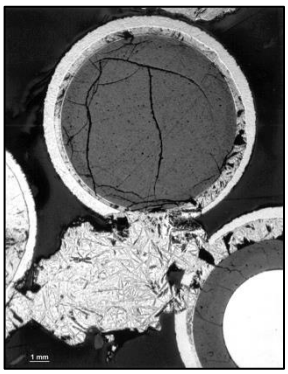

328 mm, rods 2.6 (unh.) and 1.7: min oxidised clad

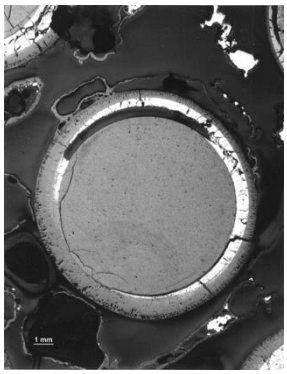

495 mm, rod 2.2: completely oxidised clad

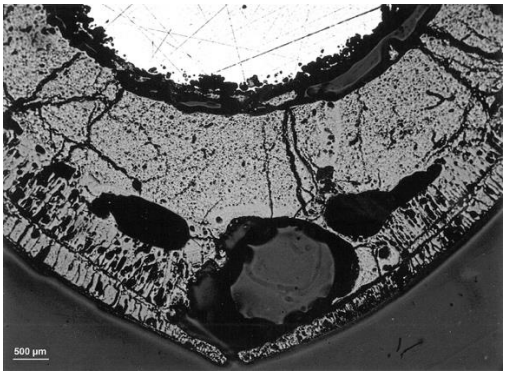

891 mm, rod 5.1: completely oxidised clad

Fig 6. CORA-15 bundle elevations between 300 and 1000 mm: cladding oxidation

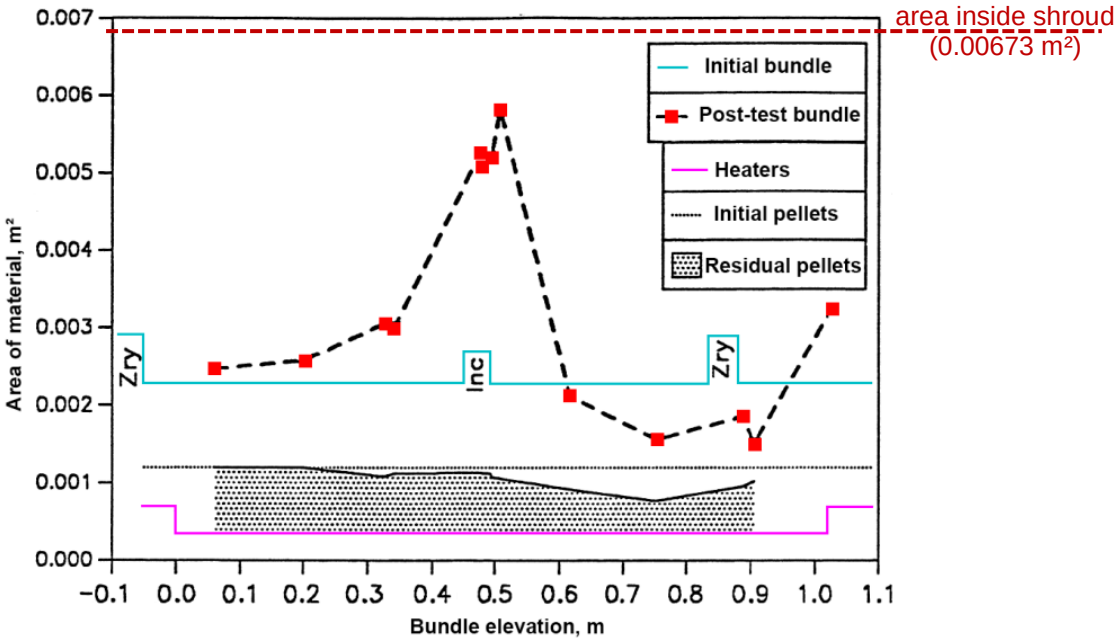

Fig 7. CORA-15: material relocation and bundle blockage

3. Simulation results

3.1. Short description of the ATHLET-CD code

The system code ATHLET-CD (Analysis of THermal-hydraulics of LEaks and Transients with Core Degradation) [10] as module of the code system AC^2 describes the reactor coolant system thermal-hydraulic response during severe accidents. It is developed by GRS in cooperation with IKE, University of Stuttgart. The code structure is highly modular to include a manifold spectrum of models and to offer an optimum basis for further development. ATHLET-CD contains the original ATHLET models for comprehensive simulation of the thermal-hydraulics in the reactor coolant system. The thermo-fluid-dynamic module is based on a six-equation model, with fully separated balance equations for liquid and vapour.

The rod module ECORE consists of models for fuel rods, absorber rods, Zr-UO_2 dissolution and melting of metallic and ceramic components. Melt relocation (candling) is simulated by rivulets with constant velocity and cross-section, starting from the node of rod failure. The models allow oxidation, freezing, re-melting, re-freezing and melt accumulation due to blockage formation. Feedback to the thermal-hydraulics considers steam starvation and blockage formation. Besides convective heat transfer, energy can be exchanged by radiation amongst fuel rods and to surrounding core structures. For the simulation of debris bed a specific model MEWA can be applied, with its own thermal-hydraulic equation system, coupled to the ATHLET fluid-dynamics on the outer boundaries of the debris bed.

3.2. Short description of the SOCRAT code

Code SOCRAT is intended for safety assessment of NPP with LWR under severe accident conditions [11]. At in-vessel stage of severe accidents, the following general processes are considered: core uncovery and heat up; radiative and convective heat transfer inside the core and between the core and surrounding in-vessel structures; deformation and burst (collapse) of fuel rod claddings; release of fission products from solid fuel into reactor coolant system (RCS); coagulation, transport and deposition/resuspension of fission products in RCS; oxidation of fuel rod claddings, absorbers and steel structures in steam or air; fuel degradation (dissolution of UO_2 and ZrO_2 by solid and molten Zr, failure of ZrO_2 protective layer; melting of oxides); fission product release from molten fuel; material relocation (formation of eutectics U-Zr-O, SS-Zr, SS-B_4C; candling down of liquid masses; collapse of fuel rods with formation of debris bed; formation and spreading of molten pools; relocation of

corium to lower plenum); oxidation of liquid metals, especially those containing liquid Zr; creep failure of RCS boundaries (hot leg nozzles, surge-line of pressurizer, SG tubes); fuel-coolant interaction in lower plenum; behaviour of molten corium inside RPV (convection; crust formation, stratification into metallic and oxide layers); degradation of lower head by molten corium impact; release of molten materials into containment after to RPV breach.

3.3. Comparison of simulations

For both codes, the rod bundle was simulated by four concentric rings according to Table 3, an inner ring (ROD1) containing the central unheated rod, a second ring containing four heated rods (ROD2), a third ring containing six unheated rods and two absorber rods (ROD3) and an outer ring with twelve heated rods (ROD4).

Rod group in code	Number of rod in the CORA-15 test bundle
Rod 1	central unheated rod (4.4)
Rod 2	inner heated rods (3.3), (3.5), (5.5), (5.3)
Rod 3	unheated rods (4.2), (2.2), (2.4), (2.6), (6.6), (6.4); *absorber rods (4.6), (6.2) in ATHLET-CD*
Rod 4	outer heated rods (1.1), (1.3), (1.5), (1.7), (3.7), (5.7), (7.7), (7.5), (7.3), (7.1), (5.1), (3.1)

Tab 3. CORA-15 rod groups for modelling

The reference time (0 s) was established for the beginning of the recording of the experiment. The reference bundle elevation (0 mm) corresponds to the bottom of the heated length in the rod simulator.

3.3.1. Cladding burst parameters for the CORA-15 bundle

Table 4 shows results of both codes concerning the burst parameters. Experimental average values of the burst time for corresponding rod groups are provided to demonstrate the burst sequence between the groups.

Unit	Description	Rod 1	Rod 2	Rod 3	Rod 4
s	time of burst $\mathbf{t_b}$	3595	3571	3612	3570
		3619	3559	3626	3593
		3601	*3559 (mean)* *3548-3564* *(time span)*	*3609 (mean)* *3565-3645* *(time span)*	*3580 (mean)* *3494-3618* *(time span)*
MPa	internal rod pressure $\mathbf{p_b}$ at predicted burst time	6.90	6.92	6.68	6.81
		6.15	5.85	6.0	5.85
		6.15	*5.44 (rod 3.3)*	*5.73 (rod 6.6)*	*5.84 (rod 7.7)*
mm	axial elevation $\mathbf{H_b}$ of middle of clad burst opening	750	750	750	750
		783	717	783	750
		not available because of the bundle melting			
°C	cladding outer temperature $\mathbf{T_b}$ at the middle of the burst at predicted burst time	767	762	766	754
		842	827	847	847
		between 650 and 850 (estimated)			
%	maximum engineering hoop strain $\boldsymbol{\varepsilon_b}$ at predicted burst time	43.64	40.97	40.55	38.87
		36	36	36	38
		not available			
MPa	azimuthal average hoop stress $\boldsymbol{\sigma_b}$ in cladding at predicted burst time	133.3	82.2	82.2	79.6
		not available			

Tab 4. Burst data calculated by ATHLET-CD, SOCRAT in comparison with *experimental results*

The corresponding comparison diagrams together with experimental data are presented in Fig. 8. Measured data that characterise the cladding burst are the burst time and the burst pressure derived from the pressure evolutions. The burst elevations are not available in the experiment because of the bundle melting in the expected ballooning zone. The burst time sequence depends mainly on the temperature distribution within the cross-section since the differences between the initial inner pressures are small. The test exhibits a large burst time span of 150 s (from 3494 to 3644 s). It indicates a large cladding temperature difference in the burst cross-sections that could be estimated as 150 K based on the measured burst time span and the heat up rate (1 K/s).

The temperature differences result from the heat losses (outer heated claddings is colder than inner ones), presence of unheated rods and absorbers as well as from a local temperature non-uniformity. The last one follows, for example, from earlier bursts of some outer heated claddings in comparison with the inner heated claddings. Averaged burst times, provided in the Table 4, indicate the following burst sequence in the test: heated inner claddings (rod 2) - outer heated claddings (rod 4) - unheated central cladding (rod 1) – inner unheated cladding (rod 3). The same tendency is predicted by both codes. The burst time span is calculated within the experimental scattering by ATHLET-CD as well as SOCRAT. Burst pressure is captured by both codes with a tendency of slight overestimation (the measured burst pressure values, provided for the groups 2-4 in the Fig. 10, were derived from the pressure evolutions of individual rods as indicated in the Table 4, not averaged over the groups).

The burst elevation could be estimated assuming that the ballooning and rupture occurred at the hottest elevation. Fig. 9 displays vertical temperature profiles at the beginning (3500 s), at the middle (3600 s) and at the end (3650 s) of the burst time span derived from all available TC readings. It allows estimation of the hottest zone location 1) between elevations 250 and 850 mm at the beginning, and 2) at an elevation of 750 mm with uncertainty bandwidth between 600 and 850 mm at the middle and at the end of burst time span. It should be noted that the cladding TC at an elevation of 750 mm indicates a lower temperature than the absorber TC at an elevation of 850 mm as one can find in Fig. 11. But the cladding TC seems to detach partially from the cladding surface since it shows the same temperature as the TC at colder shroud at the same elevation during the selected time span and even lower temperature at the later times. Estimation of the uncertainty bandwidth is based on the temperature spatial resolution.

In the numerical simulations of the test, the hottest zone was around an elevation of 750 mm throughout the burst time span. Taking into account the node sizes, the axial elevations of the clad burst openings in all rods predicted both by ATHLET-CD and SOCRAT are located between 700 and 800 mm (Fig. 8).

The burst temperatures of the unheated cladding are estimated to rise from 650 to 800 °C at the burst time span (Figs 4, 9). The heated rods are estimated to be 50 K hotter than the unheated ones based on the difference of 50 s between the mean values of the burst times shown in the Table 4. So, the estimated temperature range both for the heated and unheated rods ranges from 650 to 850 °C. The calculations with both codes lay within the estimated burst temperature band as can be found in Table 4.

Maximum engineering hoop strain achieved at the opening at the burst time is calculated by both codes as $\varepsilon_b = 100 \cdot (D_{act} - D_0)/D_0$, where Dact = $(D_{ext} + D_{in})/2$ is middle diameter of cladding, D_{ext} and D_{in}- external and internal cladding diameters at the opening at the burst time, D_0 - initial mean cladding diameter. Both codes used a simple failure criterion based on maximum strain. The difference between the predicted maximum hoop strain values (Table 4) results from different imposed values in the failure criterion.

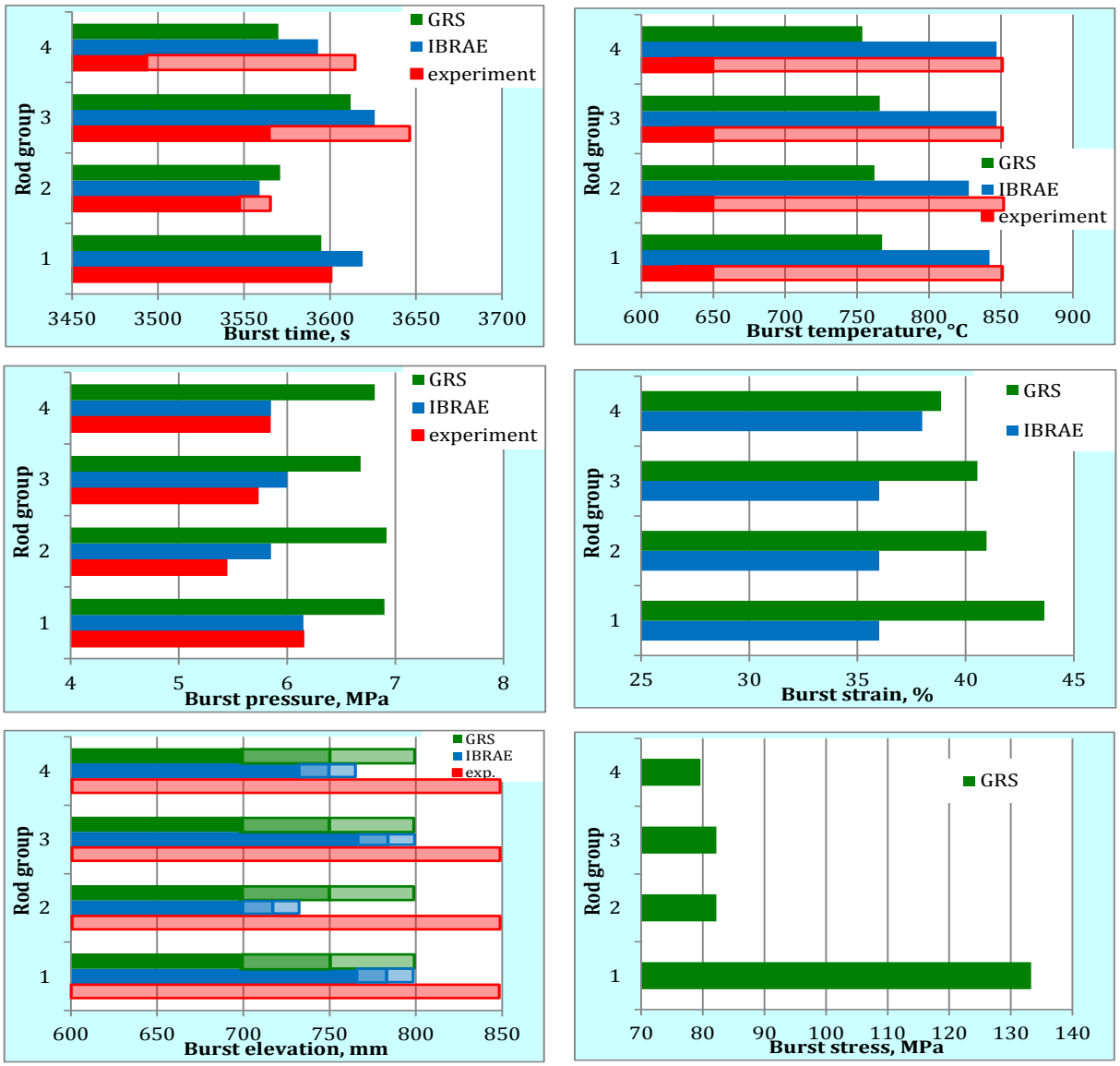

Fig 8. Burst parameters; transparent red corresponds to the measurement uncertainties, transparent green and blue - prediction due to axial node size of 100 mm (ATHLET-CD) and 33 mm (SOCRAT)

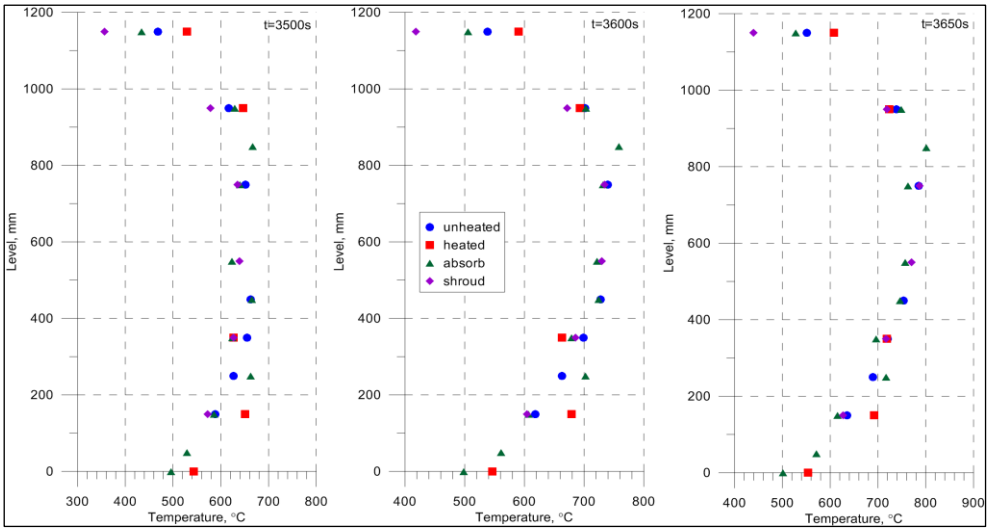

Fig 9. Vertical temperature distribution at the burst time span

3.3.2. Time dependences and axial dependences of LOCA events for central rod 4.4 of the CORA-15 bundle

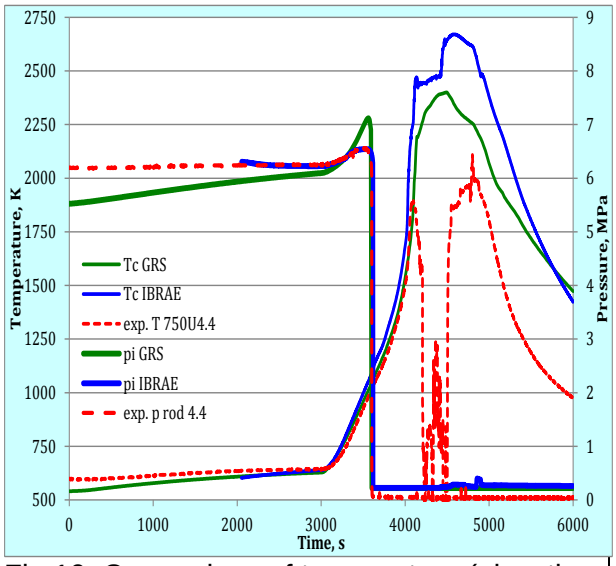

Fig 10. Comparison of temperature (elevation 750 mm) and internal pressure histories during the test

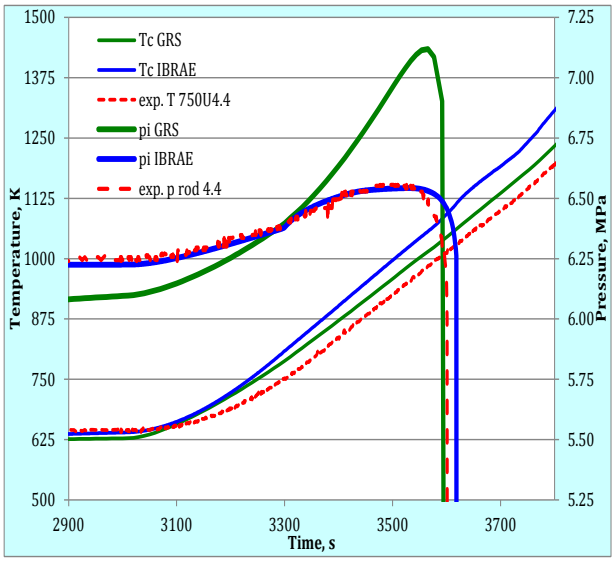

Fig 11. Comparison of temperature (elevation 750 mm) and internal pressure histories during the LOCA transient

The set of the measured burst parameters (especially temperature) are available for the central rod 4.4 only, so it was selected for the comparison. Both codes give reasonable temperature predictions at the hottest elevation – higher calculated temperatures with respect to the TC reading (Figs 10, 11) agrees with the assumption about the underestimation of cladding temperatures by TC because of its partial detachment discussed above. However, there are discrepancies in the pressure modelling: higher burst pressure for ATHLET-CD, later burst for SOCRAT.

There is a remarkable coincidence in the location and extent of the ballooning zone predicted by both codes as one can see in Fig. 12 though ATHLET-CD reveals a stronger ballooning in comparison with SOCRAT. The reason of a sharp decrease of the residual metal thickness between 450 and 950 mm is the thinning of the cladding due to ballooning. The influence of oxide layer is minimal at the burst time due to lower oxide thickness (Fig. 13). SOCRAT gives stronger oxidation (in narrower region) due to higher burst temperatures.

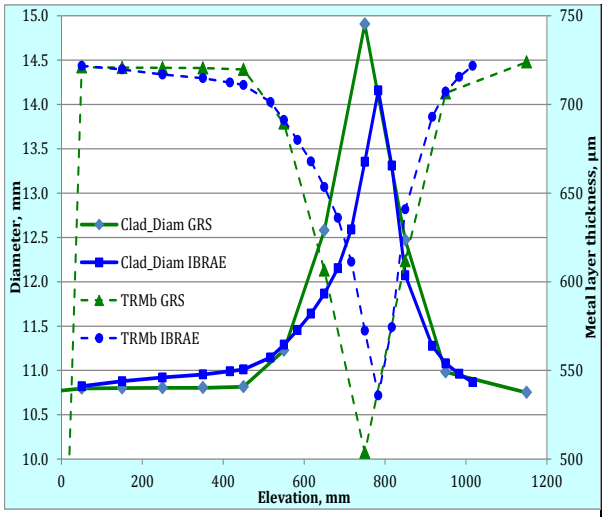

Fig 12. Axial distributions of cladding external diameter and residual metal at burst time

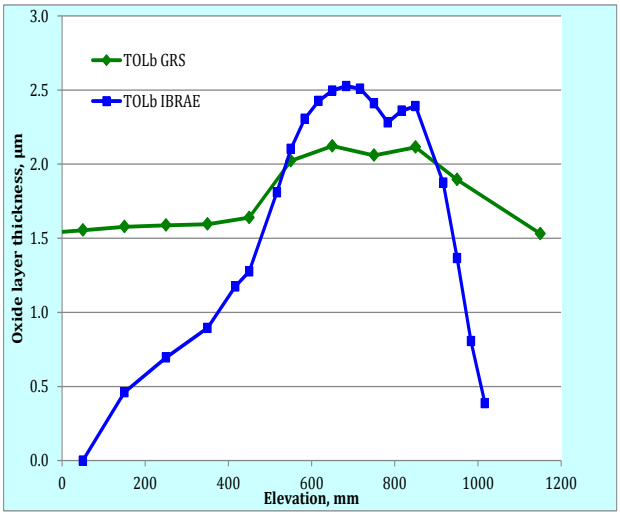

Fig 13. Axial distributions of oxide layer ZrO_2 at the outer cladding surface.

3.3.3. Post-test outer oxide layer thickness of the CORA-15 claddings

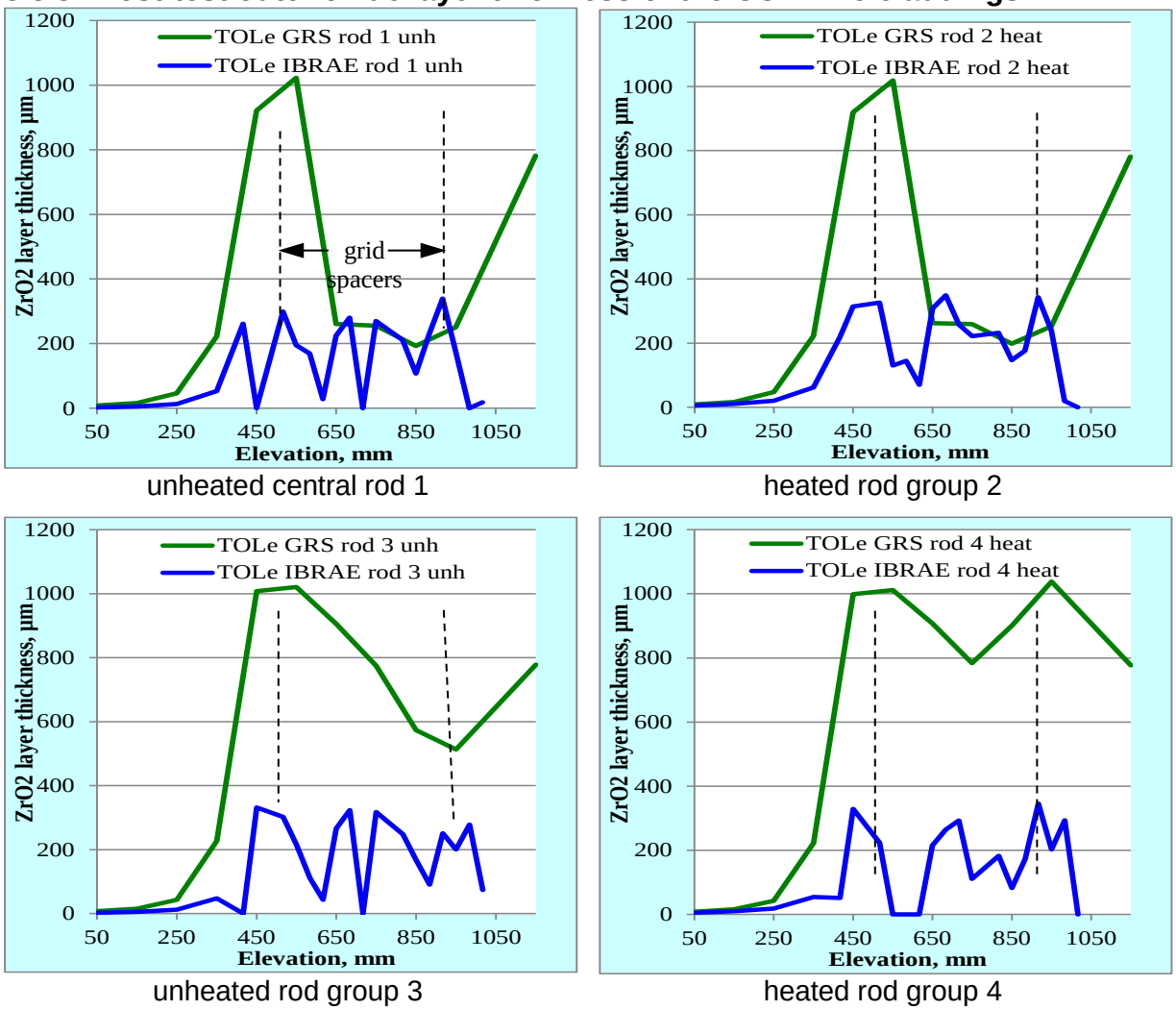

Fig 14. Results on calculated final axial distribution of oxide layer thickness at the end of the test

The parameters presented in Fig. 14 represent the thickness of ZrO_2 films «at original position» - at residuals of claddings at different elevations. They do not contain debris of the ZrO_2 relocated with the melt or any information about oxidized part of the melt. The selection of this value makes sense because it can be easily measured by rather simple optical examination of the bundle crosscuts.

Concerning the GRS data, it should be mentioned that for the central unheated rod 1 and inner heated rod group 2, the cladding metal between 650-950 mm has been completely relocated to lower elevations during the time interval 4190-4250 s. Thereafter, the thickness of residual metal at those elevations was calculated to be zero. At relocation time, oxide layer at elevation 950 mm was 251 µm. Afterwards it is kept constant, and this is the reason that it is less than the corresponding thickness at elevation 1150 mm, where the oxidation continues up to the cooling phase.

The IBRAE data shows axial variation of residual ZrO_2 thickness connected with the modelling of the start of the melt formation and its relocation through breaches of claddings. The degradation of ZrO_2 melt retention properties are governed by set of different phenomena: ballooning and burst, dissolution of oxides by molten Zr, and loss of cladding integrity due to transformation into debris.

3.3.4. Post-test blockage of the CORA-15 bundle

The bundle blockage is defined as a reduction of the area of the fluid channel:

$$B = 100 * (A_m - A_{m,\,initial}) / A_c,$$

where the area of the initial fluid channel $A_c = A_s - A_{m,\,initial} = A_s - 23*A_{rod} - 2*A_{absorber} = 0.00673 - 0.00209 - 0.0003 = 0.00434$ m² with area inside the shroud A_s=0.00673 m².

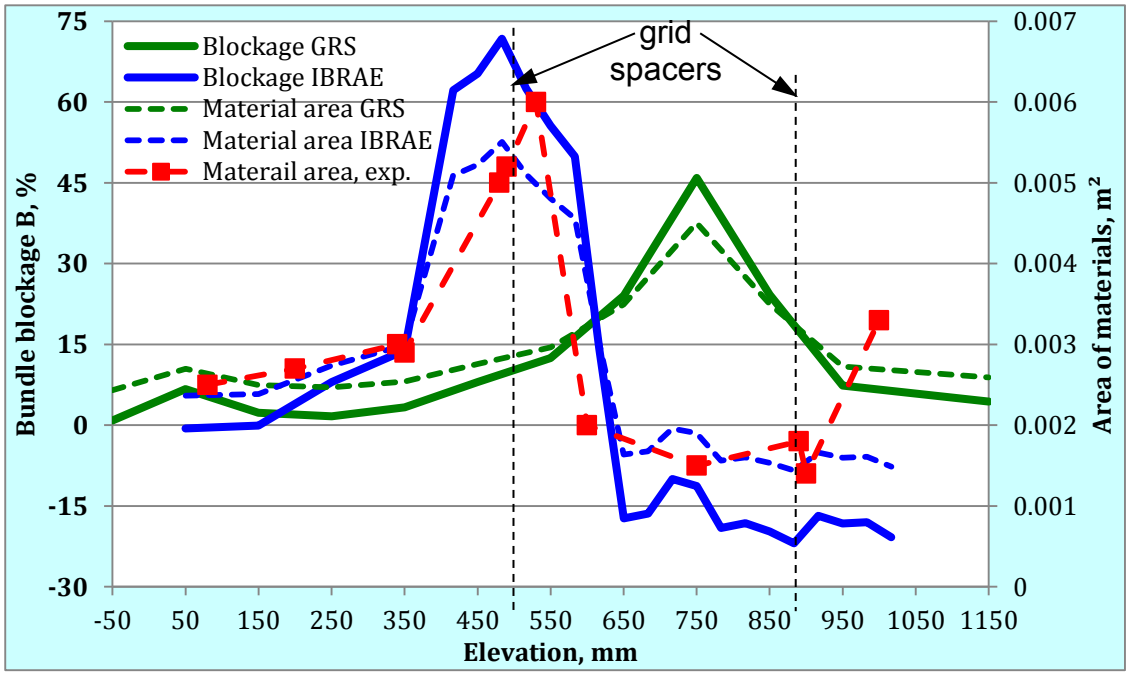

Fig 15. Results on material distribution (A_m) and bundle blockage B at the end of the test

IBRAE calculation predicts the relocation of molten materials from upper elevations to the position of the middle grid spacer (about 500 mm) that is close to the measured data as one can see in Fig. 15. For GRS, the lacking modelling of melt retention due to the spacer grids leads to an overestimation of the temperatures at elevations below the spacer grid at 450 mm. In order to artificially simulate this retention effect, a very low relocation velocity for the metallic (Zry) melt was used, which shifted the axial profile of the blockage to higher elevations.

3.3.5. Hydrogen release during the CORA-15 test

Comparison of the hydrogen flowrate and total mass calculated at the test section outlet with the data measured by two mass spectrometers located in the gas lines is presented the Figs. 16 and 17. Both codes predict the total hydrogen mass at the end of the test well (within the measurement uncertainties of one of the spectrometers). Comparison of the provided evolutions should be performed taking into account peculiarities of the gas lines with hydrogen measurement systems (effects of transport delay, dilution, mixing and so on) but they are unavailable yet. Fig. 18 shows how the hydrogen curves measured by the spectrometer after the condenser in CORA-W2 test are transformed to the hydrogen curves at the test section outlet to be compared with the calculations. So the calculated and measured hydrogen generation rates cannot be compared sure enough and Figs. 16, 17 can be used just for illustration of the modelling and facility peculiarities.

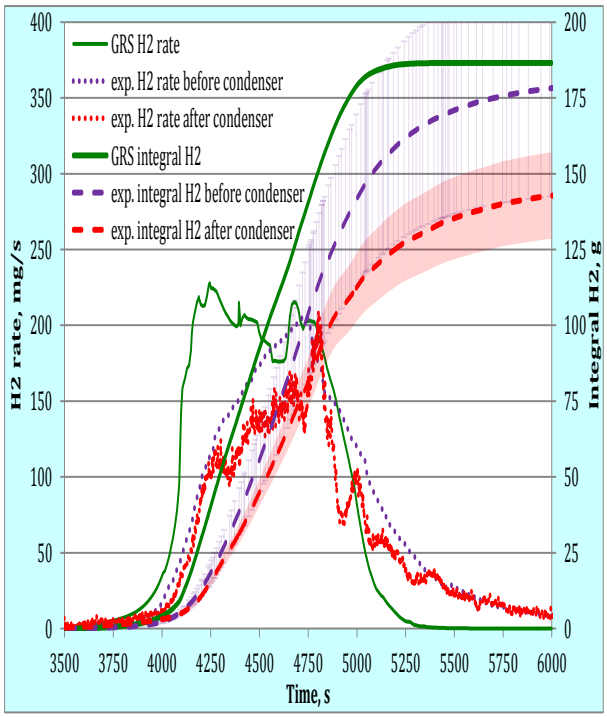

Fig 16. Comparison of GRS calculation results with experimental data of two mass spectrometers

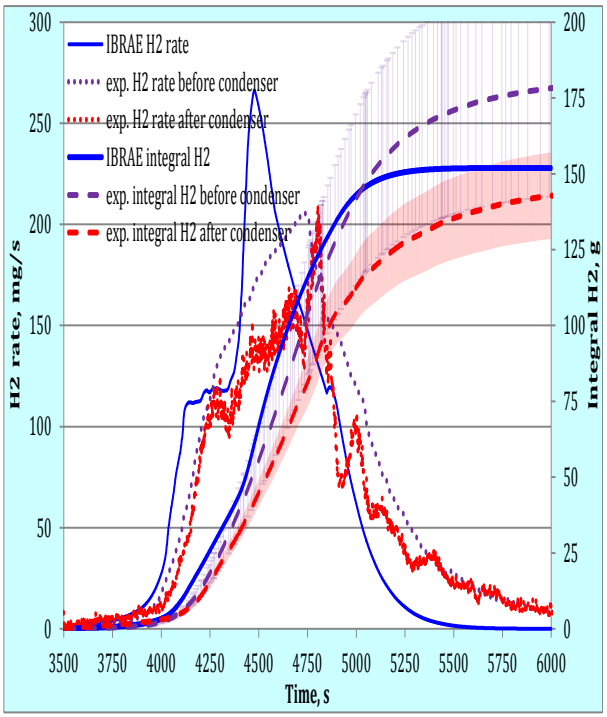

Fig 17. Comparison of IBRAE calculation results with experimental data of two mass spectrometers

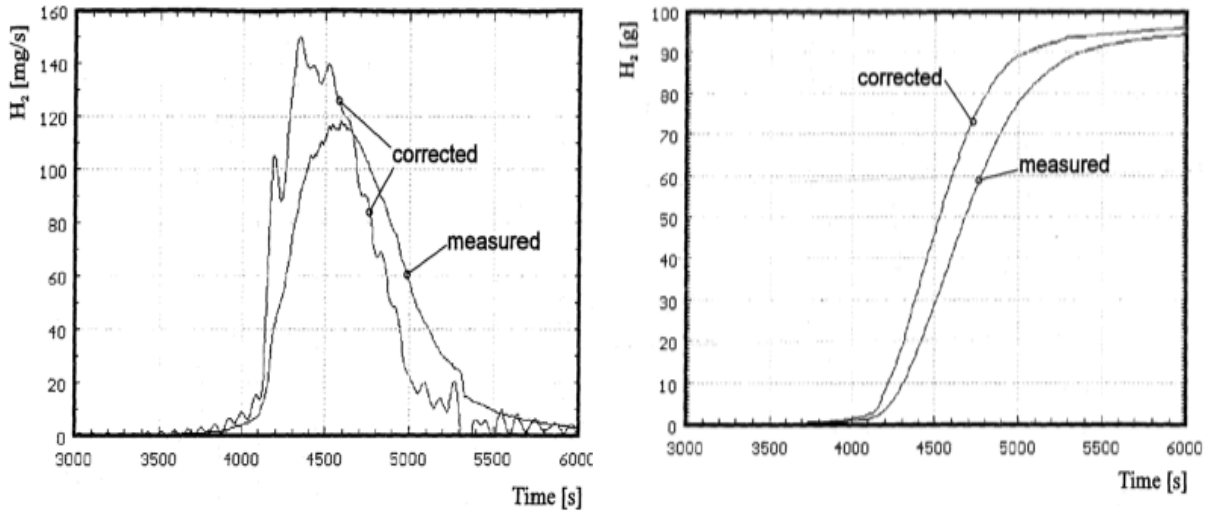

Fig 18. Effect of measurement: hydrogen production measured by spectrometer and transformed to test section outlet in CORA-W2 test [12]

4. SUMMARY AND CONCLUSIONS

The CORA-15 bundle test was performed under transient conditions typical for many CORA-PWR tests with bundle containing two Ag/In/Cd neutron absorber rods. Unlike other CORA bundles, all heated and unheated fuel rod simulators (16 + 7 correspondingly) were filled with helium and pressurized to 6.0 MPa before transient. During the transient, all rods underwent ballooning and burst. Ballooning progressed during about 100 s. Bursts occurred within 150 s (between 3500 and 3650 s) in the temperature bandwidth between about 650 and 850 °C. The mostly probable burst elevation is the bundle elevation 750 mm (the hottest elevation during the burst period).

During the further heat-up, temperature escalation due to the zirconium-steam reaction starts at elevations 550…950 mm at temperature of about 1100 °C. In presence of PWR absorber material (Ag, In, Cd) the sequence of failure starts with the release, relocation and re-solidification of the (Ag, In, Cd) melt. The absorber melt release occurred between 1290 and 1350 °C at elevations between 750 and 800 mm. Most of the melt reacts with the Zircaloy cladding and guide tube by liquefying the zirconium components, forming a metallic melt of the type (Ag, In, Zr). Due to its zirconium content this melt is capable of dissolving UO_2 as low as 1250 °C, i.e. clearly below the melting point of Zircaloy (1760 °C).

During the temperature escalation above 1800 °C, Zr melt formed in the gap between ZrO_2 and UO_2 was relocated partially inside the gap to lower bundle elevations and partially penetrated through the failed ZrO_2 layer into the space between rods. The resulting melt of the fuel rod interaction, containing mainly U, Zr, O, relocated downwards as slug and solidified between 400 and 550 mm according to its solidus temperature as a large lump of porous structure. The maximum bundle blockage (almost 100%) was observed at the top of the Inconel grid spacer (about 500 mm). The (Ag, In, Cd) absorber melt with the much lower solidus temperature solidified down at the lower elevation of about 150 mm.
Post-test investigations showed negligible oxidized cladding up to elevation of about 350 mm. The claddings were completely oxidized between elevations 480 and 1000 mm. The maximum hydrogen release rate of 210 mg/s was measured on the end of the transient (4800 s). The total hydrogen release was 145 ± 15 g.

The most recent ATHLET-CD code version has been applied for the simulation of the CORA-15 test (pressurized rods), with basically the same input data set and modelling options as for CORA-13 (not pressurized rods, subject of the IS-31 international problem). In general, a good agreement between calculated and measured data with respect to the evolution of cladding temperatures has been obtained for both tests, with a slight overestimation at the bottom and a slight underestimation at the top of the active bundle. The effect of the pressurized rods in CORA-15 has been taken adequately into account by the code. The calculated rupture time, the elevation and the cladding temperatures at burst are within the experimental ranges. The hydrogen production has been calculated within the uncertainty of the measured data, with an overestimation of the generation rate for CORA-15 during the phase of oxidation excursion between 4000 and 4500 s. One main discrepancy of the calculated results is related to the lacking modelling of melt retention due to the spacer grids, leading to a shift of the blockage profile and an overestimation of the temperatures at elevations below the spacer grids in CORA-15.

The up-to-date version V3 of SOCRAT code is applied for analyses of CORA-15 test. Set of main physical models and its parameters as well as approach to test facility nodalization are selected to be the same as usually used for LWR severe accident simulation with code validation against SET or IET data (CORA, QUENCH, PARAMETER, PHEBUS, etc.). From the comparison of the results of CORA-15 modelling with the measured data one can conclude that SOCRAT code quantitatively reproduces the claddings temperature evolution with a tendency of a slight overestimation of the cladding temperatures at the top of the heated length. The calculated burst parameters (times, pressures, elevations, and temperatures), the total hydrogen mass, the blockage formation due to melt relocation and solidification match to data well taking into account the accuracy of the measurements.

In general, the post-test simulation of the CORA-15 test allows drawing conclusions that the measured data are rather well consisted (temperature behaviour, burst parameters, total hydrogen production, post-test degradation status of bundle). The analysis performed by two system severe accident codes, ATHLET-CD and SOCRAT, reveal a good compliance with the measured data as well as with each other.

5. REFERENCES

[1] Peter Hofmann, Siegfried J. L. Hagen, Volker Noack, Gerhard Schanz, Leo K. Sepold „Chemical-physical behaviour of light water reactor core components tested under severe reactor accident conditions in the CORA facility", Nucl. Tech. 118 (1997), pp. 200-224, DOI: 10.13182/NT118-200, https://doi.org/10.13182/NT118-200.

[2] M. Firnhaber, K. Trambauer, S. Hagen, P. Hofmann: "ISP-31 – OECD/NEA-CSNI International Standard Problem No. 31 – CORA-13 Experiment on Severe Fuel Damage", GRS Report GRS-106, KfK 5287, NEA/CSNI/R(93) 17, July 1993, https://publikationen.bibliothek.kit.edu/270036036/3813515.

[3] W. Hering, „Modellierung des Experimentes Cora und Interpretation von Versuchsergebnissen mit dem erweiterten Kernschmelzcode SCDAP/MOD1", Dissertation, University of Stuttgart, IKE 2-100, 1993, https://www.tib.eu/de/suchen/id/TIBKAT%3A126025266/Modellierung-des-Experimentes-Cora-und-Interpretation/.

[4] W. Hering, P. Hofmann: „Material Interactions during Early-Phase Core Melt Progression", Festschrift Energie-Technik-Umwelt, Prof. Dr. Unger, RUB Bochum, May 1994.

[5] L. Sepold, S. Hagen, P. Hofmann, G. Schanz, "Behavior of AgInCd absorber material in Zry/UO_2 fuel rod simulator bundles tested at high temperatures in the CORA facility". Scientific report FZKA-7448, January 2009, https://publikationen.bibliothek.kit.edu/270074441/3815428.

[6] M. S. Veshchunov, J. Stuckert, A. V. Berdyshev, "Modelling of Zr-O and U-Zr-O melts oxidation and new crucible tests". Scientific report FZKA-6792, December 2002, https://publikationen.bibliothek.kit.edu/270053667/3814311.

[7] T. Haste, M. Steinbrück, M. Barrachin, O. de Luze, M. Grosse, J. Stuckert, "A comparison of core degradation phenomena in the CORA, QUENCH", Phébus SFD and Phébus FP experiments. Nuclear Engineering and Design, Volume 283, March 2015, Pages 8-20, https://doi.org/10.1016/j.nucengdes.2014.06.035.

[8] VESHCHUNOV, M. S., BOLDYREV, A. V., SHESTAK, V. E. Modelling the formation and oxidation of molten pools. Annals of Nuclear Energy, Volume 61, November 2013, Pages 54-62, https://doi.org/10.1016/j.anucene.2013.03.046.

[9] M. S. Veshchunov, V. E. Shestak, "Model for melt blockage (slug) relocation and physico-chemical interactions during core degradation under severe accident conditions", Nuclear Engineering and Design, Volume 238, Issue 12, December 2008, Pages 3500-3507, https://doi.org/10.1016/j.nucengdes.2008.08.012.

[10] H. Austregesilo et al.: "ATHLET-CD 3.1A – User's Manual", GRS Report GRS-P-4/Vol. 1, July 2016

[11] L. Bolshov and V. Strizhov, "SOCRAT – The System of Codes for Realistic Analysis of Severe Accidents". Proc. of ICAPP'06. Reno, NV USA, June 4–8, 2006, http://www.ans.org/store/item-700324/.

[12] S. Hagen, P. Hofmann, V. Noack, G, Schanz et al. "Behavior of VVER-1000 Fuel Element with Boron Carbide/Steel Absorber Tested under Severe Fuel Damage Conditions in the CORA Facility. (Results of Experiment CORA-W2)". KfK 5363, 1994, https://publikationen.bibliothek.kit.edu/270036514/3813519